AUS: Anisotropic undrained shear strength model for clays

K. Krabbenhøft[a,*], S.A. Galindo-Torres[a], X. Zhang[a], J. Krabbenhøft[b]

[a] *School of Engineering, University of Liverpool, UK*
[b] *Optum Computational Engineering, Copenhagen, Denmark*
[*] *Email: kristian.krabbenhoft@liverpool.ac.uk*

Abstract

A total stress model applicable to clays under undrained conditions is presented. The model involves three strength parameters: the undrained shear strengths in triaxial compression, triaxial extension and simple shear. The amount of physical anisotropy implied by the model is a function of the relative magnitude of these three strengths assuming a Mises type plastic potential. Elastoplastic deformation characteristics below failure are accounted for by a hardening law requiring two additional parameters that can be related to the axial strains halfway to failure in triaxial compression and extension. Finally, elasticity is accounted for by Hooke's law. The result is a relatively simple model whose parameters can all be inferred directly from a combination of in-situ and standard undrained laboratory tests. The model is applied to a problem involving the horizontal loading of a monopile foundation for which full scale tests previously have been conducted. The model shows good agreement with the measured data.

Key words: Clay, undrained shear strength, Generalized Tresca, anisotropy, monopiles.

1 INTRODUCTION

Many geotechnical problems may be analyzed assuming undrained conditions. That is, under the assumption that the dissipation of the excess pore pressures generated in response to loading is negligible during the time period of interest, e.g. the period of construction or the period from load application to possible failure. For such problems, it is common practice to model the material behaviour with reference to total, rather than effective, stresses. The simplest possible elastoplasticity model within the total stress framework is the linear elastic-perfectly plastic Tresca model which involves two parameters: the undrained Young's modulus (or the shear modulus) and the undrained shear strength, both of which may be specified to vary with depth. While crude, this model does – with careful selection of the two parameters – offer a reasonable estimate of both the defor-

mation characteristics under working conditions and the strength characteristics at the ultimate limit state.

Somewhat surprisingly, while there have been significant advances in the development of constitutive models for clays based on the more rigorous and arguably theoretically more satisfactory effective stress approach, total stress models have evolved little beyond the aforementioned linear elastic-perfectly plastic Tresca model. Considering that a number of salient features are not captured by this model, there appears to be scope for an extension of these types of linear elastic-perfectly plastic models, analogous in many ways to the extension of such models in the more general effective stress setting.

This paper is concerned with one such extension. Following the conventional constitutive modeling paradigm, the model, denoted AUS (Anisotropic Undrained Shear strength model), is based on elastoplasticity. Rather than the standard Tresca strength criterion, the so-called Generalized Tresca criterion is used. This strength criterion involves two parameters, namely the undrained shear strengths in triaxial compression and extension, and may be shown to be consistent with the effective stress Mohr-Coulomb model under undrained conditions [7]. The Generalized Tresca model pertains to isotropic materials, i.e. materials that have the same properties in all directions. The unequal strengths in compression and extension implied by the model is essentially a Lode angle effect and is not due to physical anisotropy, i.e. different properties in different directions.

The AUS model extends the Generalized Tresca model to anisotropic materials, in particular to the case of cross anisotropy, stemming for example from a preferential direction of deposition. However, the two effects – Lode angle dependence and anisotropy – are clearly delineated and treated separately. Secondly, in contrast to the linear elastic-perfectly plastic Tresca models (standard as well as Generalized), the AUS model incorporates plasticity prior to failure. This is achieved by means of a hardening Generalized Tresca yield surface involving two parameters that can be related to the axial strain at half the failure stress in triaxial compression and extension. These parameters can, together with the undrained shear strengths, be inferred directly from experiments. As such, the model is straightforward to calibrate as will be demonstrated with respect to a number of experimental data sets.

2 FAILURE CRITERION

The theoretical motivation for the classic linear elastic-perfectly plastic total stress models is as follows. Assuming that the stiffness of the soil skeleton is much smaller than the stiffness of both the pore fluid and the soil grains, it may be shown [e.g. 11] that the change in volume as a result of undrained loading is negligible. For a linear elastic-perfectly plastic effective stress models, this implies that the change in effective mean stress is zero regardless of the loading programme. In this way, analysis in terms of total rather than effective stresses becomes possible. For the Mohr-Coulomb criterion with cohesion c and

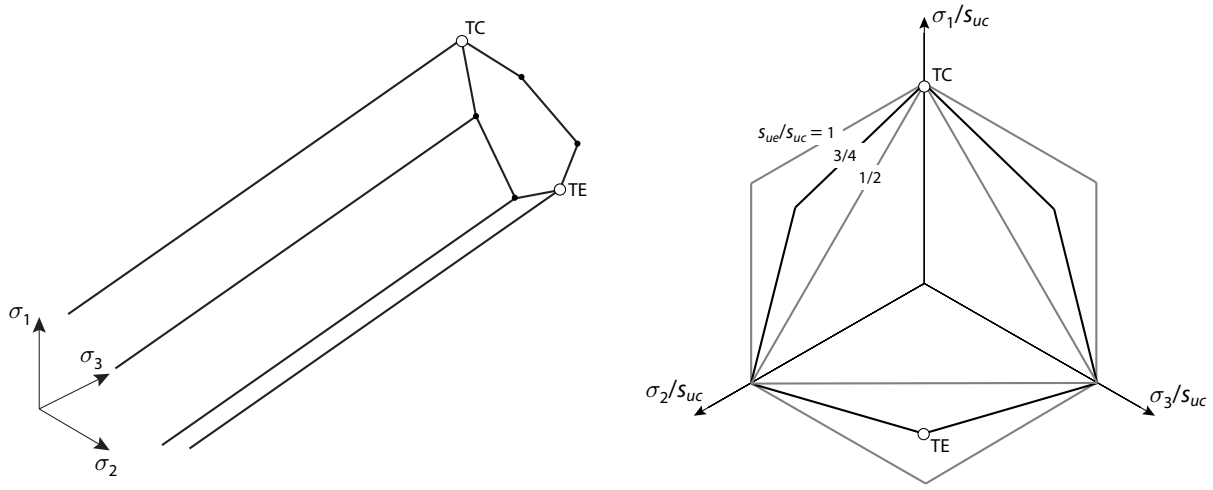

Fig. 1. Generalized Tresca failure surface in principal stress space (left) and in the deviatoric plane (right). The points indicated correspond to triaxial compression (TC) and triaxial extension (TE).

friction angle ϕ:

$$F = \sigma_1 - \sigma_3 - (\sigma'_1 + \sigma'_3)\sin\phi - 2c\cos\phi = 0 \tag{1}$$

it has been shown [7] that the equivalent total stress, or undrained, failure criterion is given in terms of the so-called Generalized Tresca criterion [1]:

$$F_u = \sigma_1 - \sigma_3 + \left(\frac{s_{uc}}{s_{ue}} - 1\right)(\sigma_2 - \sigma_3) - 2s_{uc} = 0 \tag{2}$$

where $\sigma_1 \geq \sigma_2 \geq \sigma_3$ are the principal stresses (positive in compression) and

$$\begin{aligned} s_{uc} &= \frac{3\sin\phi}{3 - \sin\phi}\left(p'_0 + \frac{c}{\tan\phi}\right) \\ s_{ue} &= \frac{3\sin\phi}{3 + \sin\phi}\left(p'_0 + \frac{c}{\tan\phi}\right) \end{aligned} \tag{3}$$

are the undrained shear strengths in triaxial compression and extension respectively, p'_0 being the initial effective mean stress. The Generalized Tresca criterion depicts a pressure insensitive prism with a hexagonal cross section in principal stress space (see Figure 1). The undrained shear strengths are limited by

$$\frac{1}{2} \leq \frac{s_{ue}}{s_{uc}} \leq 1 \tag{4}$$

Outside this range, the failure surface is non-convex.

Assuming a von Mises plastic potential (which will be used later on), it may be shown that the undrained strength in simple shear ($\dot{\varepsilon}^p_1 = -\dot{\varepsilon}^p_3$, $\dot{\varepsilon}^p_2 = 0$ at the ultimate limit state)

[1] Correcting an error of sign in [7].

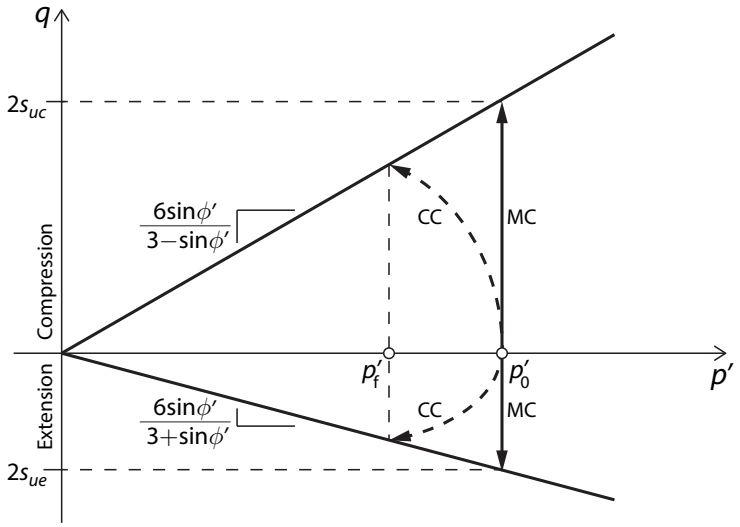

Fig. 2. Response of common soil models for normally consolidated clays under undrained conditions: linear elastic-perfectly plastic Mohr-Coulomb (MC) and Cam clay type models (CC). The undrained shear strengths indicated are those consistent with the former model.

is given by

$$s_{us} = \left[\frac{1}{2}\left(\frac{1}{s_{ue}} + \frac{1}{s_{uc}}\right)\right]^{-1} = \frac{2s_{ue}s_{uc}}{s_{ue} + s_{uc}} \tag{5}$$

That is, as the harmonic mean of the compression and extension strengths. As such, s_{us} is always closer to s_{ue} than to s_{uc}.

The underlying Mohr-Coulomb model leading to the undrained shear strengths (3) is based on a number of assumptions (perfect plasticity, zero dilation, etc) that often are in contradiction with experimental data. In particular, normally consolidated clays have a tendency to contract as a result of shearing, leading to a decrease in effective mean stress and thereby a decrease in undrained shear strength as compared to what is implied by the Mohr-Coulomb model. This effect is captured by more advanced models such as the Cam clay models and their later extensions [see e.g. 11]. Many such models operate under the classic critical state premise which under undrained conditions implies that the effective mean stress at failure is given uniquely by the initial effective mean stress and the model parameters, regardless of the path along which failure is reached (see Figure 2). As such, use of the Generalized Tresca model to capture failure is still justified as long as the undrained shear strengths (3) are adjusted appropriately to reflect that the effective mean stress does not remain constant but instead reaches a unique terminal value at failure (shown as p'_{f} in Figure 2).

More generally, rather than construct an effective stress constitutive model to account in detail for the physics eventually leading to a given undrained shear strength, the idea with the total stress models is to operate directly with the measured undrained shear strengths. As such, while the above relations provide some motivation for how an appropriate total stress model may be constructed, they are not in any way fundamental.

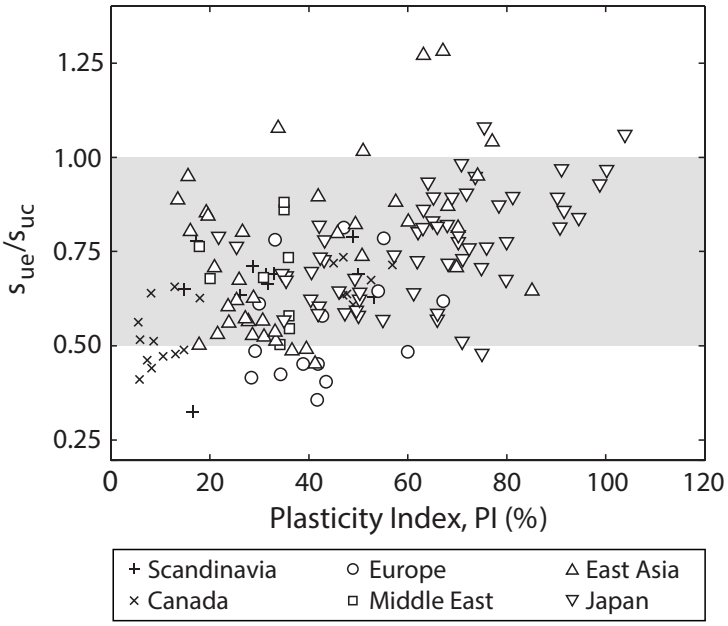

Fig. 3. Experimental data of s_{ue}/s_{uc} ratios versus plasticity index collated by [18]. The shaded region indicates the range of validity of the Generalized Tresca model ($0.5 \leq s_{ue}/s_{uc} \leq 1$)

However, considering that clays usually display different undrained strengths in compression and extension (see Figure 3), it appears reasonable to operate with a total stress model capable of capturing this basic feature. In other words, while the standard Tresca model involving a single strength parameter often is used, the Generalized Tresca model (which contains the standard model as a special case) appears rather more appropriate. The Generalized Tresca model is compared to a set of triaxial tests conducted by [12] in Figure 4. While the agreement is not perfect, it does provide a better fit than single parameter models such as Tresca and von Mises. It is also noted that the von Mises circles provide a reasonable fit to the measured directions of plastic strain rate in the deviatoric plane. Hence, von Mises will be used as plastic potential in the following.

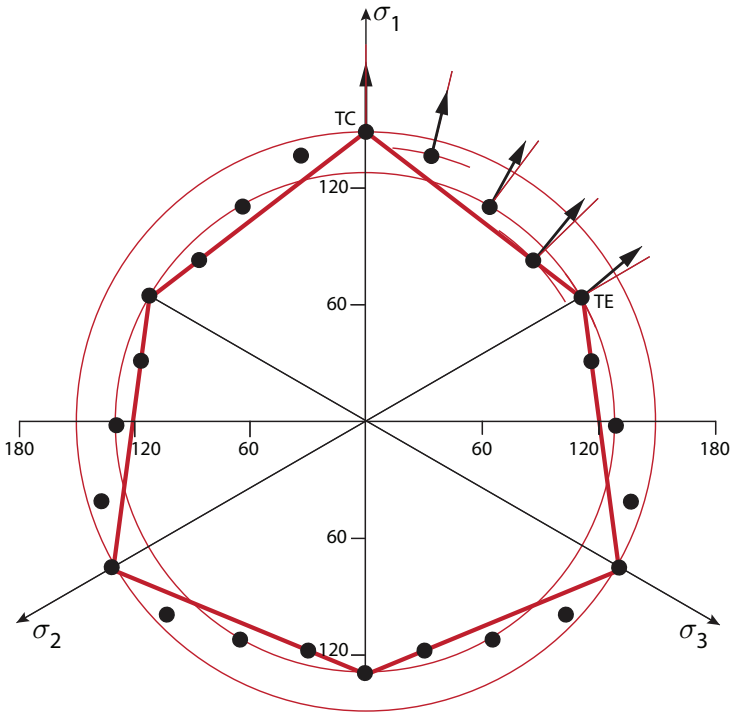

Fig. 4. Generalized Tresca failure surface and Mises circles matched to triaxial compression and extension along with undrained true triaxal data for normally consolidated kaolin clay [12] at an effective mean stress of 160 kPa. The ratio between the undrained shear strengths in extension and compression is $s_{ue}/s_{uc} \approx 0.87$. The arrows indicate the measured plastic strains which are compared to those implied by the circular von Mises plastic potential.

2.1 Anisotropy

The characteristic of unequal shear strengths in triaxial compression and extension is often referred to as 'anisotropy' [e.g. 4; 5; 10]. This is rather unfortunate as unequal compression and extension strengths is an inherent feature of ideal isotropic Mohr-Coulomb materials, c.f. the previous section. On the other hand, it is obviously conceivable that natural clays, due to their deposition, stress history, etc, would display a certain amount of strength anisotropy, i.e. would have different strengths when subjected to the same loading programme at two different angles relative to a given plane of anisotropy.

In the following, a model incorporating cross-anisotropic strength, stemming for example from a preferential direction of deposition, is considered. Identifying the normal to the plane of anisotropy (the direction of deposition) as the z-direction, the strength anisotropy may, following Grimstad et al. [4], be accommodated by an appropriate shift of the yield surface. In the case where all shear stresses are zero, the geometric interpretation is a shift of the Generalized Tresca surface in the direction of the σ_z axis (see Figure 5). The additional degree-of-freedom required to accommodate this shift may be related to the undrained shear strength in simple shear on the plane of anisotropy. In the following, in order to avoid an excessive number of subscripts, we will make reference to material

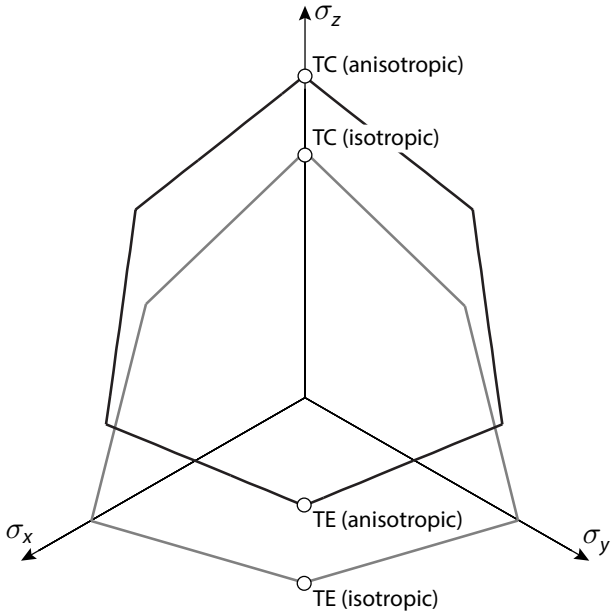

Fig. 5. Shift of the Generalized Tresca surface to accommodate specified s_{ue}/s_{uc} and s_{us}/s_{uc} ratios in the case where all shear stresses are zero.

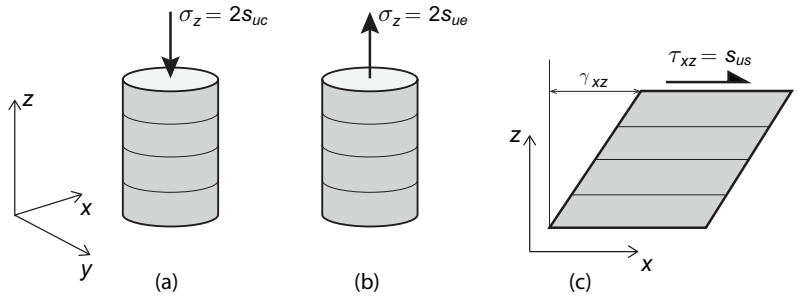

Fig. 6. Tests associated with strength parameters: (a) triaxial compression ($\sigma_z > \sigma_x = \sigma_y$), (b) triaxial extension ($\sigma_z < \sigma_x = \sigma_y$) and simple shear ($\gamma_{xy} > 0$ and all other strains equal to zero). The plane of anisotropy is normal to the z-axis.

parameters s_{uc} and s_{ue} to denote the undrained shear strengths measured in triaxial compression and extension, respectively, for a sample that is oriented such that the load is applied normal to the plane of anisotropy. Similarly, s_{us} refers to the simple shear strength for a sample sheared on the plane of anisotropy. The three different tests are sketched in Figure 6.

In the general case, the relevant anisotropic version of the Generalized Tresca model may be written as (again following [4] and using standard continuum mechanics sign conventions):

$$F_u = \hat{q} - \frac{6k}{\sqrt{3}(1+1/\rho)\cos\hat{\theta} - 3(1-1/\rho)\sin\hat{\theta}} \tag{6}$$

where

$$\hat{q} = \sqrt{3\hat{J}_2} \tag{7}$$

$$\hat{J}_2 = \tfrac{1}{2}\hat{\boldsymbol{s}}^{\mathsf{T}}\boldsymbol{D}\hat{\boldsymbol{s}} \tag{8}$$

$$\hat{\boldsymbol{s}} = \boldsymbol{\sigma} - \boldsymbol{m}p - ak\boldsymbol{r} \tag{9}$$

$$\boldsymbol{m} = (1,1,1,0,0,0)^{\mathsf{T}} \tag{10}$$

$$\boldsymbol{D} = \mathrm{diag}(1,1,1,2,2,2) \tag{11}$$

$$p = \tfrac{1}{3}\boldsymbol{m}^{\mathsf{T}}\boldsymbol{\sigma} \tag{12}$$

$$\boldsymbol{r} = (\tfrac{1}{3},\tfrac{1}{3},-\tfrac{2}{3},0,0,0)^{\mathsf{T}} \tag{13}$$

$$\hat{\theta} = \tfrac{1}{3}\arcsin\left(\frac{3\sqrt{3}}{2}\frac{\hat{J}_3}{\hat{J}_2^{3/2}}\right) \tag{14}$$

$$\hat{J}_3 = \hat{s}_{xx}\hat{s}_{yy}\hat{s}_{zz} + 2\hat{s}_{xy}\hat{s}_{yz}\hat{s}_{zx} - \hat{s}_{xy}^2\hat{s}_{zz} - \hat{s}_{yz}^2\hat{s}_{xx} - \hat{s}_{zx}^2\hat{s}_{yy} \tag{15}$$

and k, ρ, and a are material parameters. Geometrically, these are related to the size, shape and shift of the yield surface respectively. For $k = s_{uc}$, $\rho = s_{ue}/s_{uc}$ and $a = 0$, the original Generalized Tresca surface (2) is recovered. In the general anisotropic case, k, ρ and a may be related to the three undrained shear strengths, s_{uc}, s_{ue} and s_{us} by

$$k = \frac{1 + s_{ue}/s_{uc}}{1+\rho}s_{uc} \tag{16}$$

$$a = 2\frac{\rho - s_{ue}/s_{uc}}{1 + s_{ue}/s_{uc}} \tag{17}$$

$$\rho = \frac{s_{ue} + s_{uc} - s_{us} - \sqrt{(s_{ue}+s_{uc})(s_{ue}+s_{uc}-2s_{us})}}{s_{us}} \tag{18}$$

These relations all rely on the plastic strains following from the flow rule:

$$\dot{\boldsymbol{\varepsilon}}^p = \dot{\lambda}\frac{\partial G}{\partial \boldsymbol{\sigma}} \tag{19}$$

where G is a von Mises type potential given by

$$G = \hat{q} \tag{20}$$

That is, a Mises cylinder shifted by the same amount as the Generalized Tresca failure surface. This type of flow potential has both been observed experimentally in true triaxial tests [12, see also Figure 4] and has a long history in the modeling of clays, going back at least to the work of Roscoe and Burland [14] on Modified Cam Clay.

The condition that the yield surface remains convex ($\frac{1}{2} \le \rho \le 1$) imposes the following limitations on s_{us}/s_{uc} as function of s_{ue}/s_{uc}:

$$\frac{4}{9}\left(1 + \frac{s_{ue}}{s_{uc}}\right) \le \frac{s_{us}}{s_{uc}} \le \frac{1}{2}\left(1 + \frac{s_{ue}}{s_{uc}}\right) \tag{21}$$

The lower limit here corresponds to a Rankine triangle in the deviatoric plane while the upper limit corresponds to a Tresca hexagon. The admissible parameter range is shown in Figure 7 along with experimental data of Ladd [10] and Karlsrud and Hernandez-Martinez

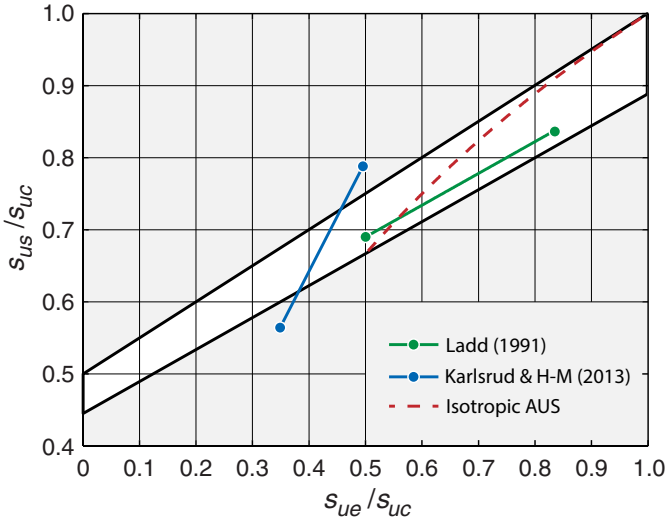

Fig. 7. Admissible parameter space for AUS model together with experimental data of Ladd [10] and Karlsrud and Hernandez-Martinez [5]. The isotropic version of the AUS model (no shift of the yield surface) is also indicated.

[5] (see also Appendix 1).

It should be noted that the above expressions imply $\rho = s_{ue}/s_{uc}$ for a simple shear strength equal to that of the isotropic model, $s_{us} = 2s_{ue}s_{uc}/(s_{ue}+s_{uc})$. In that case, there is no shift of the yield surface ($a = 0$). In other words, anisotropy only results from input (s_{uc}, s_{ue}, s_{us}) that cannot be accommodated by the original isotropic Generalized Tresca model. This is a natural consequence of the fact that the model involves three parameters, or 'degrees-of-freedom', k, ρ, and a, that can be related uniquely to the three undrained shear strengths. While more degrees-of-freedom could be added to control for example a rounding of the Generalized Tresca surface, this would imply a loss of the uniqueness between the model parameters and the undrained shear strengths and thereby necessitate a number of deliberate and possibly less than obvious choices.

2.2 Plane strain

For the important special case of plane strain ($\dot{\varepsilon}_y^p = 0$ at the ultimate limit state), the yield function is given by

$$F = \sqrt{(\sigma_z - \sigma_x + ak)^2 + 4\tau_{zx}^2} - \frac{4\rho}{1+\rho}k \tag{22}$$

which reduces to the standard plane strain Tresca yield function for $s_{ue} = s_{uc} = s_{us} = s_u$ (corresponding to $a = 0$, $\rho = 1$, $k = s_u$).

For the isotropic version of the model [$s_{us} = 2s_{ue}s_{uc}/(s_{ue}+s_{uc})$], we have $a = 0$, $\rho = s_{ue}/s_{uc}$

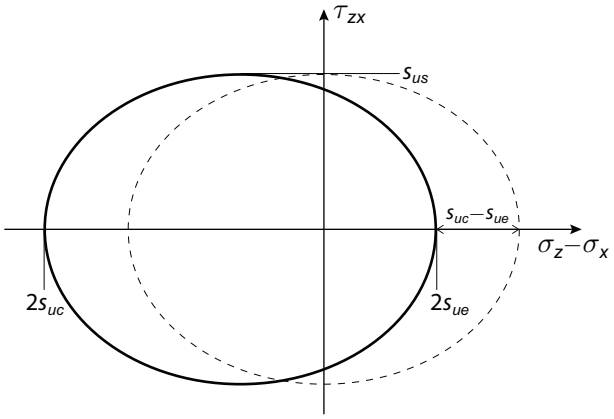

Fig. 8. AUS yield surface in plane strain (stresses negative in compression) for $s_{us} = \frac{1}{2}(s_{ue}+s_{uc})$ (24).

and $k = s_{uc}$ and thereby

$$F = \sqrt{(\sigma_z - \sigma_x)^2 + 4\tau_{zx}^2} - 2s_{us} \tag{23}$$

In other words, the 'effective' undrained shear strength is that measured in simple shear.

Another interesting special case is that where $s_{us} = \frac{1}{2}(s_{uc} + s_{ue})$. The yield function is here given by

$$F = \sqrt{(\sigma_z - \sigma_x + s_{uc} - s_{ue})^2 + 4\tau_{zx}^2} - 2s_{us} \tag{24}$$

That is, an ellipse of magnitude with axes $s_{ue}+s_{uc}$ and s_{us} shifted by and amount $s_{uc}-s_{ue}$ along the $(\sigma_z - \sigma_x)$-axis (see Figure 8).

2.3 Evaluation of anisotropy

The basic premise of the model presented above is that anisotropy is indirectly characterized by the three undrained shear strengths s_{uc}, s_{uc} and s_{us} measured as shown in Figure 6. For combinations that cannot be accounted for using the isotropic Generalized Tresca surface, anisotropy results. That is, for $s_{us} = 2s_{ue}s_{uc}/(s_{ue} + s_{uc})$, the model is isotropic while for all other ratios some amount of anisotropy is necessary to account for all three strengths.

In the following, we examine the effects of this anisotropy in more detail. In doing so, we focus on the important special case where

$$s_{us} = \tfrac{1}{2}(s_{ue} + s_{uc}) \tag{25}$$

This is a common approximation [see e.g. 13] and corresponds to the upper boundary of the admissible parameter space shown in Figure 7.

Consider now the situation where a sample has been taken out of the ground, trimmed appropriately and then subjected to a state of biaxial compression at an angle α relative

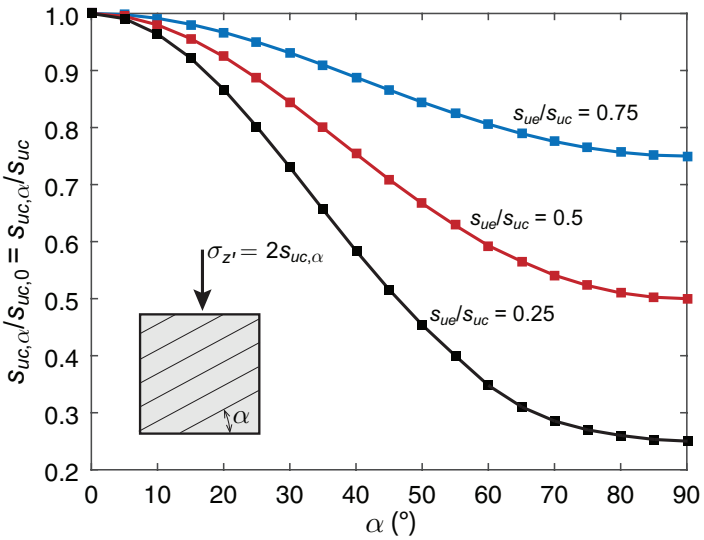

Fig. 9. Undrained strength as function of load inclination relative to the plane of anisotropy for different s_{ue}/s_{uc} and $s_{us} = \frac{1}{2}(s_{uc} + s_{uc})$.

to the plane of anisotropy (see Figure 9). For $\alpha = 0°$ the sample is loaded normal to the plane of anisotropy and the strength is $s_{uc,0} = s_{uc}$ while for $\alpha = 90°$ the sample is loaded parallel to the plane of anisotropy and the measured strength is $s_{uc,90} = s_{ue}$.

The results are shown in Figure 9. These have been computed numerically using the program OptumG2 [8] which implements the model. The strength dependence on the angle of inclination is, qualitatively, similar to previously reported experimental results [see e.g. 11]. This type of variation is predicted by other relevant clay models including the NGI-ADP [4] and MIT-E3 [17] models.

3 HARDENING LAW

Hardening is specified by first replacing the quantity k in the expression for the failure surface (26) by a hardening variable κ:

$$F_u = \hat{q} - \frac{6\kappa}{\sqrt{3}(1 + 1/\rho)\cos\hat{\theta} - 3(1 - 1/\rho)\sin\hat{\theta}} \tag{26}$$

By making κ vary from some initial value, κ_0, such that the initial stress state, $\boldsymbol{\sigma}_0$, satisfies $F(\boldsymbol{\sigma}_0, \kappa_0) = 0$ to an ultimate value of $\kappa = k$, a family of affine surfaces are generated for each value of κ between $\kappa = \kappa_0$ and $\kappa = k$ (see Figure 10). This type of isotropic hardening is obviously just one possibility. In monotonic loading, it does not differ essentially from other types of hardening whereas the modeling of cyclic loading would require a more careful consideration of the exact type of hardening (isotropic, kinematic, mixed, etc).

As for the exact functional form of the hardening law, we have been inspired by the work

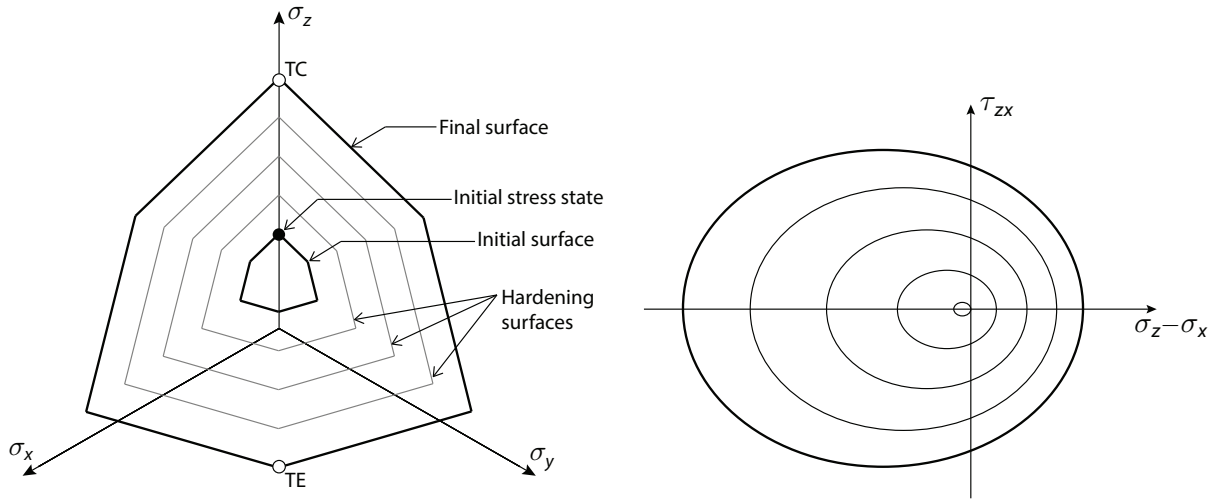

Fig. 10. Hardening AUS yield surfaces in the deviatoric plane (left) and in plane strain (right).

of Vardanega and Bolton [16] who, on the basis of a large data base of triaxial test results, proposed the following power law relation between deviatoric stress, q and axial strain, ε_a:

$$\frac{q}{2s_{uc}} = \frac{1}{2}\left(\frac{\varepsilon_a}{\beta}\right)^{\alpha} \tag{27}$$

where α and β are model parameters. We see that β in fact is the axial strain at half the mobilized strength, i.e. for $q/2s_{uc} = \frac{1}{2}$. As for the parameter α, Vardanega suggested a value of 0.6 but other, though similar, values are often appropriate. The relation (27) is illustrated in Figure 11.

Assuming that the initial stress is at the yield surface initially such that $q = 2\kappa$ throughout and making the quite reasonable assumption that the total strain is governed by the plastic strain, we have

$$\frac{q}{2s_{uc}} = \frac{\kappa}{s_{uc}} = \frac{\kappa}{k} = \frac{1}{2}\left(\frac{\varepsilon_a^p}{\beta}\right)^{\alpha} \tag{28}$$

The rate form of (28) is given by

$$\dot{\kappa} = h_1 \dot{\varepsilon}_a^p = \dot{\lambda} h_1 \tag{29}$$

where $\dot{\lambda}$ is the plastic multiplier and

$$h_1 = \frac{\alpha k}{2\varepsilon_a^p}\left(\frac{\varepsilon_a^p}{\beta}\right)^{\alpha} = \frac{\alpha k}{2\beta}\left(\frac{2\kappa}{k}\right)^{\frac{\alpha-1}{\alpha}} \tag{30}$$

Somewhat of a disadvantage of the above hardening law is that κ needs to be capped explicitly. That is, κ does not approach k asymptotically but rather increases indefinitely with the strain (see also Figure 11). This shortcoming is addressed by the following law:

$$\kappa = k\left(1 - 2^{-\varepsilon_a^p/\beta}\right) \tag{31}$$

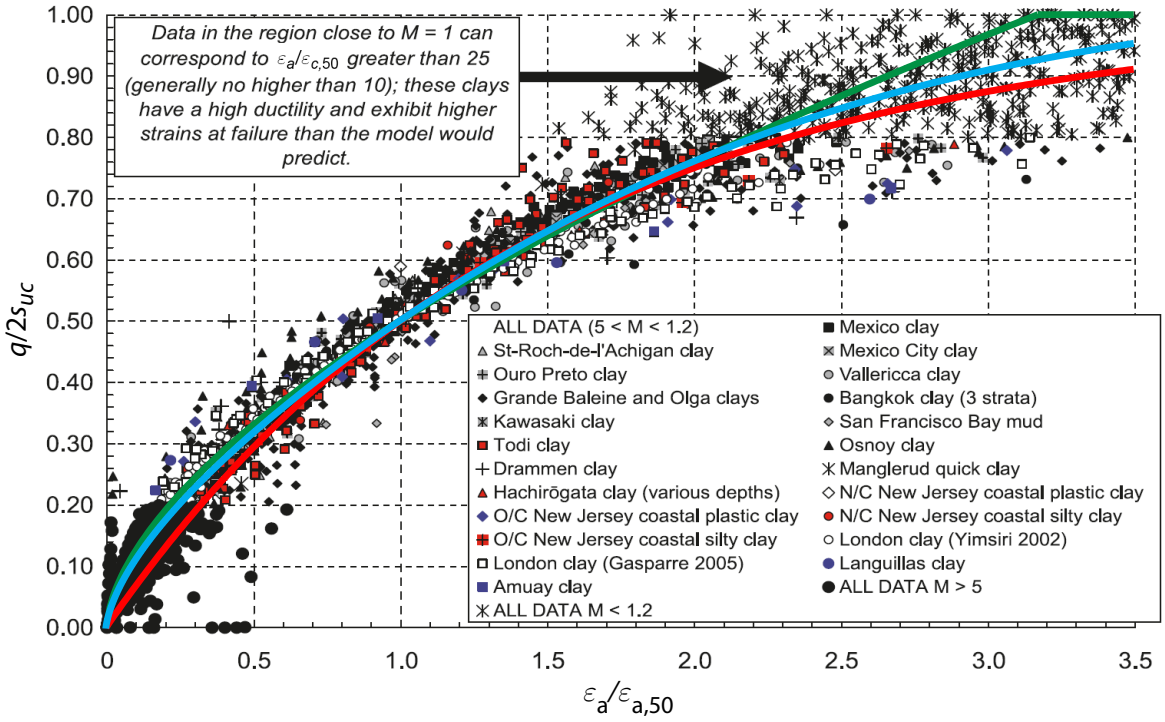

Fig. 11. Relative mobilized strength versus relative strain for the hardening laws (28) (green), 31 (red), and 34 (blue). According to [16], the scatter around the pivot point $(\varepsilon_a/\varepsilon_{a,50}, q/2s_{uc}) = (1, \frac{1}{2})$ is due to errors digitizing previously published data or noise in the original data. After [16]. © 2011 Canadian Science Publishing or its licensors. Reproduced with permission.

where β again is the strain at half the mobilized strength. The rate form of the above law is given by:

$$\dot{\kappa} = \dot{\lambda} h_2 \tag{32}$$

where

$$h_2 = \frac{k \ln 2}{\beta} 2^{-\varepsilon_a^p/\beta} = \frac{\ln 2}{\beta}(k - \kappa) \tag{33}$$

While the alternative law (31) does have the correct asymptotic behaviour at large strains, it implies a less stiff response at small strains than the Vardanega-Bolton law (see also Figure 11). Hence, we opt for a compromise law given by

$$\dot{\kappa} = \dot{\lambda} h \tag{34}$$

where

$$h = (1 - \kappa/k) h_1 + \kappa/k h_2 \tag{35}$$

such that h_1 dominates for small strains while h_2 dominates for larger strains.

In the general case, the parameter β may be taken as

$$\beta = \left(\frac{1}{2} - \frac{\sqrt{3}}{2}\tan\hat{\theta}\right)\varepsilon_{c,50}^p + \left(\frac{1}{2} + \frac{\sqrt{3}}{2}\tan\hat{\theta}\right)\varepsilon_{e,50}^p \tag{36}$$

where $\varepsilon^p_{c,50}$ and $\varepsilon^p_{e,50}$ are two new material parameters, namely the axial plastic strains halfway to failure in triaxial compression ($\hat{\theta} = -30°$) and triaxial extension ($\hat{\theta} = +30°$) respectively.

4 ELASTICITY

The last remaining component of the model is the elastic law relating elastic strains to total stresses. Assuming linear elasticity we have

$$\boldsymbol{\varepsilon}^e = \mathbb{C}_u \boldsymbol{\sigma} \tag{37}$$

where the undrained elastic compliance modulus is given by:

$$\mathbb{C}_u = \frac{1}{3G_0} \begin{bmatrix} 1 & -\frac{1}{2} & -\frac{1}{2} & & & \\ -\frac{1}{2} & 1 & -\frac{1}{2} & & & \\ -\frac{1}{2} & -\frac{1}{2} & 1 & & & \\ & & & 3 & & \\ & & & & 3 & \\ & & & & & 3 \end{bmatrix}$$

with G_0 being the shear modulus ($E_u = 3G_0$ being the undrained Young's modulus).

The use of isotropic elasticity for materials with anisotropic strength characteristics is arguably somewhat unsatisfactory. However, for most problems of practical interest, plasticity rather than elasticity is expected to be dominant. As such, and in the interest of simplicity, the present version of the AUS model operates with isotropic elasticity.

5 MODEL CALIBRATION

Two model calibrations are performed in the following. Since no data for s_{us} was provided, the isotropic version of the AUS model is used [$\rho = s_{ue}/s_{uc}$ and thereby $s_{us} = 2s_{ue}s_{uc}/(s_{ue} + s_{uc})$].

5.1 Isotropically consolidated triaxial compression test

In the following the AUS model is calibrated to a set of triaxial compression data obtained by [1]. The material, a natural intact Todi clay, was isotropically consolidated to various pressures and then subjected to undrained triaxial compression. For the data considered

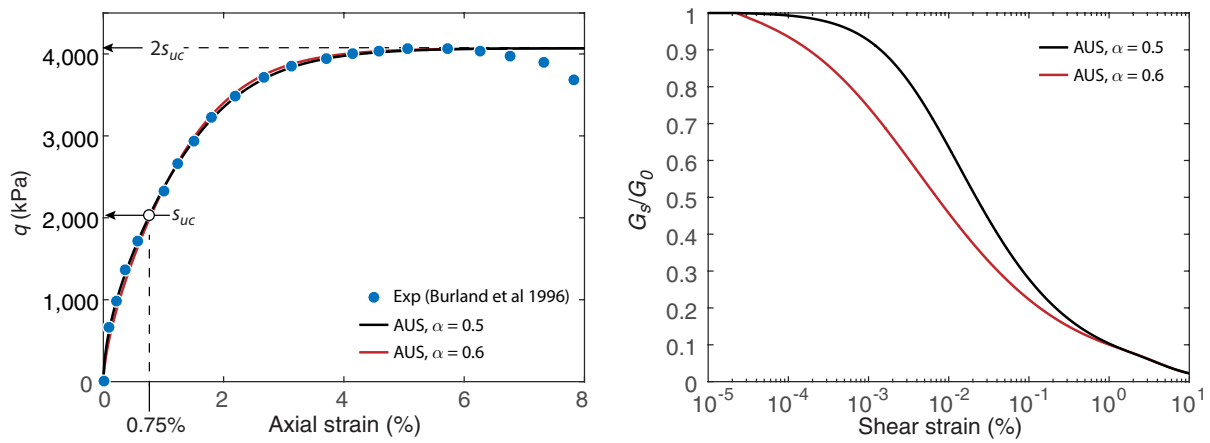

Fig. 12. AUS fit to Burland et al. [1] data.

in the following the initial confining pressure was $p'_0 = 3,200\,\text{kPa}$.

The calibration of the model proceeds as follows. First the undrained shear strength is read off as $s_{uc} = 0.5(\sigma_1 - \sigma_3)_{\max} \approx 2,035\,\text{kPa}$. Next, the axial strain at half the failure load is identified as $\varepsilon_{c,50} \approx 0.75\%$. Most of the deformation up to this level is assumed to be plastic and hence we set $\varepsilon^p_{c,50} = 0.75\%$ in the AUS model. Finally, the undrained Young's modulus is taken as 10 times the secant stiffness modulus $E_{50,c} = s_{uc}/\varepsilon_{50}$. That is, $E_u = 3G = 2,710\,\text{MPa}$. The fit shown in Figure 12 then results. We see that the parameter α affects the response primarily at small strains while at large strains the exact value of the parameter is relatively inconsequential. The remaining parameters (which have no influence on the behaviour in compression) must either be estimated or derived from additional extension and simple shear tests. It should be noted that both s_{uc} and, to a lesser extent, $\varepsilon_{c,50}$, are pressure dependent. Vardanega and Bolton [16] have proposed a number of relations accounting for this and other effects. Finally, the AUS model does not include strain softening. As such, the apparent softening observed in the experimental results in Figure 12 cannot be captured.

5.2 K_0 consolidated triaxial compression and extension tests

Next, the model is fitted to triaxial compression and extension tests for a silty clay conducted by Won [19]. The data are plotted in Figure 13. For the compression test, the initial stress state was $(\sigma'_1, \sigma'_3)_0 = (65.4\,\text{kPa}, 46.1\,\text{kPa})$ while for the extension test it was $(\sigma'_1, \sigma'_3)_0 = (56.4\,\text{kPa}, 44.7\,\text{kPa})$. The undrained shear strengths, identified immediately from the data, are $s_{uc} = 13.3\,\text{kPa}$ and $s_{ue} = 9.2\,\text{kPa}$. The axial strains halfway to failure in compression and extension are estimated at $\varepsilon_{c,50} = 1\%$ and $\varepsilon_{e,50} = 3\%$. Finally, the undrained Young's modulus is set to $E_u = 10\,\text{MPa}$. For these model parameters, the AUS fits are as shown in Figure 13. While the fits are less than perfect, the model does reproduce the overall features of the stress-strain behaviour. It should be noted that the fits to a large extent are influenced by the choice of fixing the size of the initial yield

surface to pass through the initial stress point. For the extension test, this means that the initial stress state is at a compression corner (similar to what is shown in Figure 10). Once the extension test commences, a substantial elastic region then needs to traversed before yielding is recorded in extension. For the present test, this means that the stiffness at intermediate stress levels in extension is somewhat overestimated.

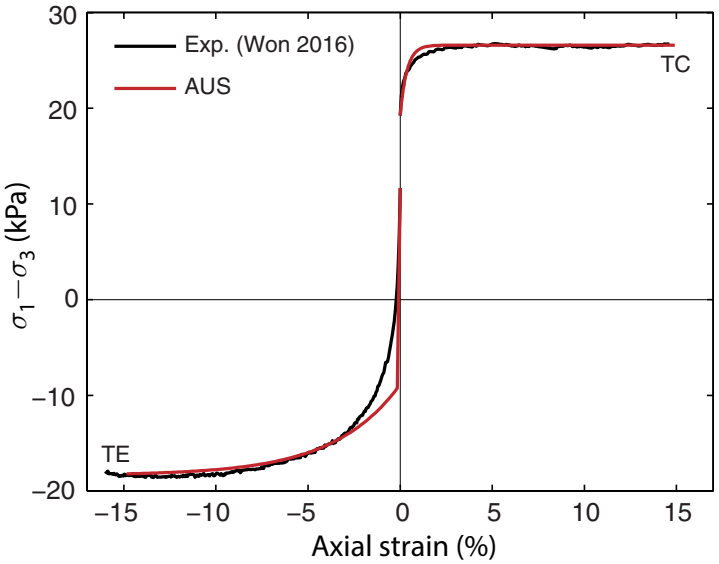

Fig. 13. AUS fits to triaxial compression (TC) and extension (TE) tests of Won [19].

6 ANALYSIS OF MONOPILE FOUNDATION

In the following, the AUS model in applied to the analysis of a monopile subjected to horizontal loading. All data, including the measured response, are from the so-called PISA project [2; 3; 20] which involved full scale tests on a variety of monopiles of different dimensions, depths, pile wall thickness, etc. From partial data published, it is possible to infer full sets of problem data for a number of particular cases. One such case is the one sketched in Figure 14.

The steel monopile has a total length of 17.6 m, a diameter of 0.762 m and a wall thickness of 25 mm. The penetration into the soil is 7.6 m and the loading is applied 10 m above the ground surface. The adopted profiles of triaxial compression undrained shear strength (s_{uc}), elastic shear modulus (G), and coefficient of earth pressure at rest (K_0) are shown in Figure 15. The effective unit weight is taken as $\gamma' = 11.4\,\mathrm{kN/m^3}$. To examine the effects of the deformation parameters $\varepsilon^p_{c,50}$ and $\varepsilon^p_{e,50}$, two load-displacement analyses are conducted: one for $\varepsilon^p_{c,50} = 0.5\%$ and one for $\varepsilon^p_{c,50} = 0.25\%$. In both cases, $\varepsilon^p_{e,50}/\varepsilon^p_{c,50} = 4$.

Regarding the s_{uc}/s_{ue} ratio, Zdravkovic et al. [20] report drained triaxial compression and extension angles of $\phi_c = 27°$ and $\phi_c = 32°$ respectively. The analysis of Section 2 thus

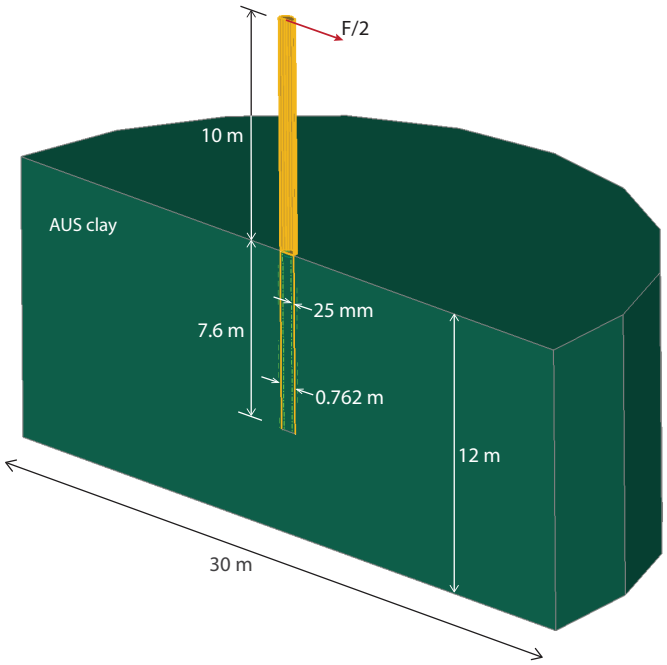

Fig. 14. Monopile subjected to horizontal loading.

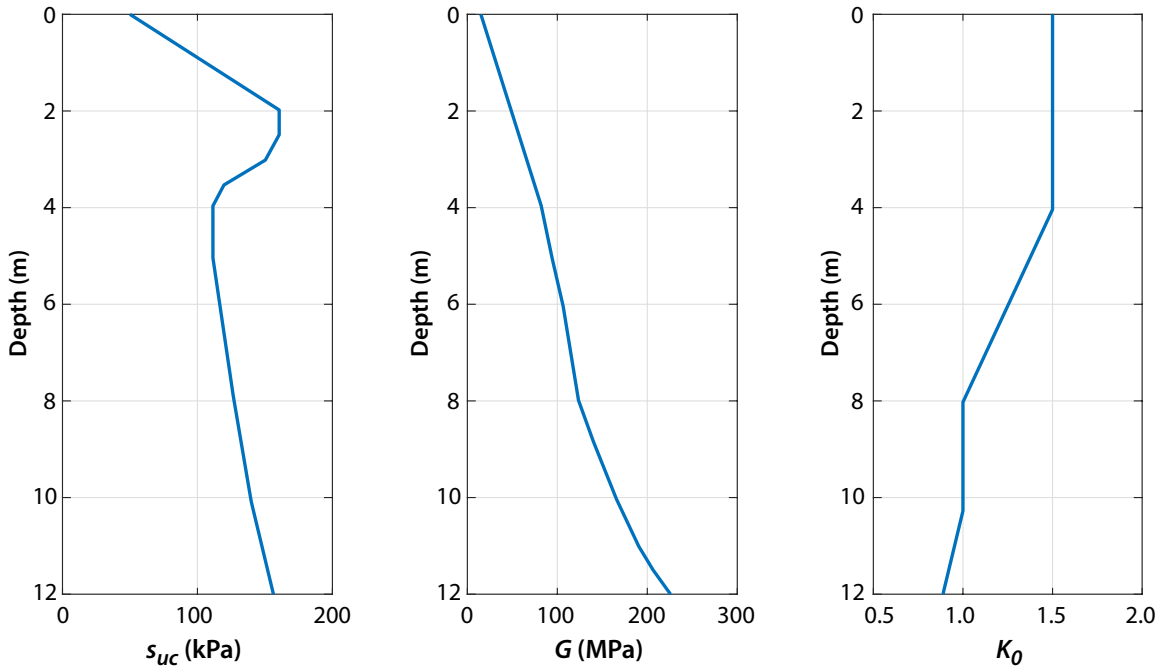

Fig. 15. Adopted profiles of triaxial compression undrained shear strength (s_{uc}), elastic shear modulus (G), and coefficient of earth pressure at rest (K_0). The two former are from [2] and the latter is from [20].

suggests a ratio of

$$\frac{s_{ue}}{s_{uc}} = \frac{3 - \sin\phi_c}{3 + \sin\phi_e}\frac{\sin\phi_e}{\sin\phi_c} = 0.84 \tag{38}$$

which, without additional data, may be taken as the best estimate of true ratio.

The pile is assumed elastic with $E = 210\,\text{GPa}$ and $\nu = 0.3$ and is modelled using shell elements. At the interface between the clay and the pile, a tension cut-off is used. Following Zdravkovic et al. [20], the undrained shear strength at the interface is assumed equal to that of the surrounding soil. While some amount of reduction of interface shear strength is required by most codes of practice, we have generally found that the closest match with measured data is achieved by maintaining the full shear strength at the interface.

Symmetry is utilized so that only one half of the problem is modelled as shown in Figure 14. All analyses are conducted with the finite element program OptumG3 [9]. While the s_{ue}/s_{uc} ratio of 0.84 calculated on the basis of the drained friction angles is not unreasonable and falls well within the range of ratios regularly observed (see Figures 3 and 7), it is entirely possible that the true ratio would be different. Hence, to assess the effects of the s_{ue}/s_{uc} ratio, limit analyses are conducted for s_{ue}/s_{uc} in the range of 0.2 to 1.0. In all cases, the simple shear strength is taken as $s_{us} = \frac{1}{2}(s_{ue} + s_{uc})$, implying a degree of anisotropy that decreases as s_{ue}/s_{uc} increases towards $s_{ue}/s_{uc} = 1$ in which case the standard Tresca failure criterion is recovered.

The results are shown in Figure 16. It is seen that the capacity to a very good approximation is a linear function of s_{ue}/s_{uc} or, alternatively, of s_{us}/s_{uc} within the range considered. Indeed, the failure load can be reasonably approximated by

$$F = \frac{s_{us}}{s_{uc}} F_1 \tag{39}$$

where F_1 is the failure load for $s_{ue}/s_{uc} = s_{us}/s_{uc} = 1$. The linear dependency of ultimate capacity on s_{us}/s_{uc} is unique to this particular problem, but illustrates a more general point that analyses on the basis of the triaxial compression strength alone, e.g. using the standard Tresca model, may overpredict the capacity significantly.

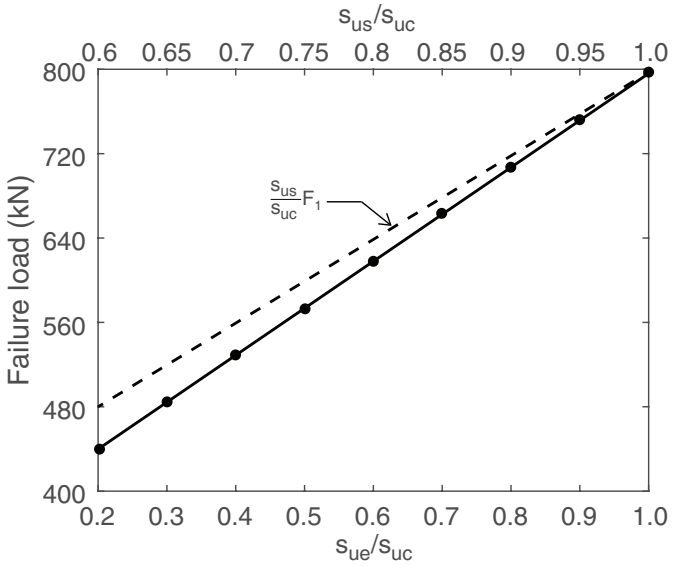

Fig. 16. Failure load versus shear strength ratio.

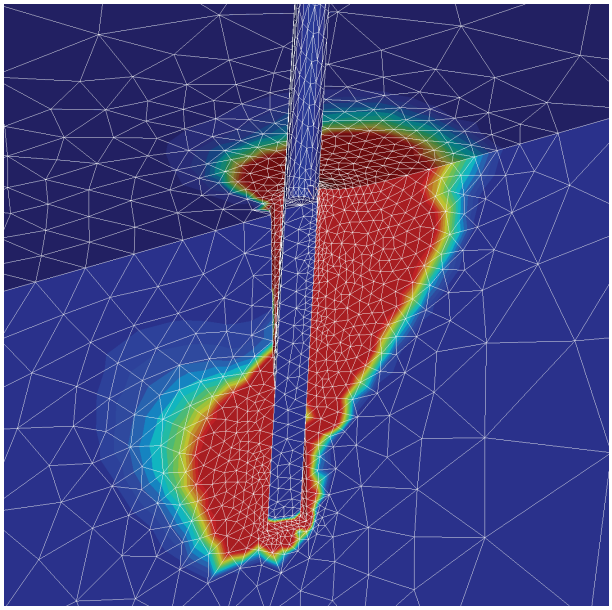

Fig. 17. Shear strain distribution at failure.

Finally, a load-displacement analysis is conducted for the best estimate of the parameters of $s_{ue}/s_{uc} = 0.84$. Again, the simple shear strength is set to $s_{us} = \frac{1}{2}(s_{ue} + s_{uc}) = 0.92 s_{uc}$. This implies a slight anisotropy as compared to the isotropic version of the model where $s_{us} = 2s_{uc}/(1 + s_{uc}/s_{ue}) = 0.91 s_{uc}$. The horizontal displacement of the pile at ground level are shown in Figure 18. We see a relatively stiff response initially followed the expected decrease in stiffness as the yield zone around the pile spreads. It should be noted that the ultimate limit state is reached only at very large deformations – larger than can be justified in a standard small-deformation analysis such as the present one. Indeed, a displacement at the ground level of $0.1D$ corresponding to nominal failure [2; 20], is reached already at about half the failure load.

The two analyses with $\varepsilon^p_{c,50} = 0.25\%$ and $\varepsilon^p_{c,50} = 0.5\%$ appear to bracket the test re-

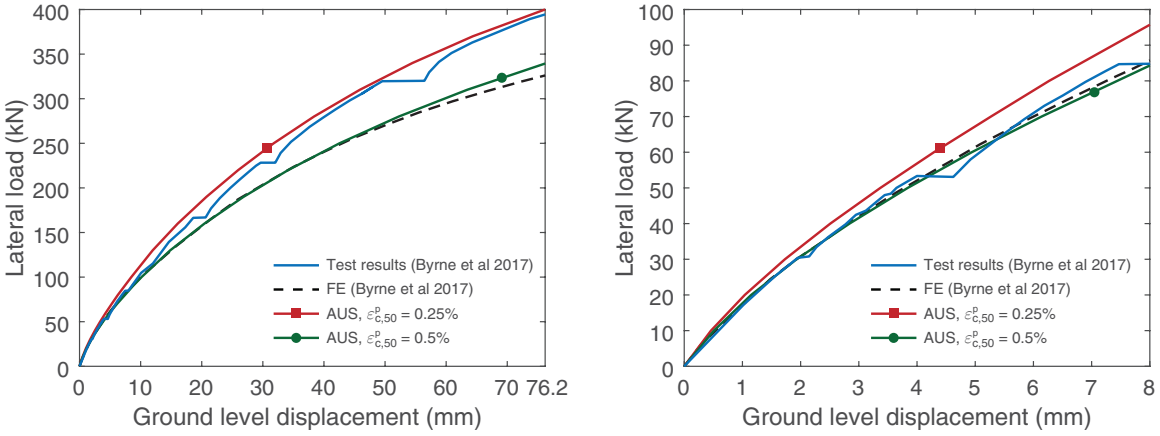

Fig. 18. Load-displacement curves at ground level with zoom of the conditions at small displacements (right).

sults fairly well. Somewhat of a complication, however, is that the tests were conducted with regular interruptions where creep and excess pore pressure dissipation was allowed to progress. These periods appear as the approximately horizontal segments of the load-displacement curve and are followed by a stiffer response consistent with an increase of strength as a result of an increase in effective mean stress and thereby in undrained strength. Finally, the analysis with $\varepsilon^p_{c,50} = 0.5\%$ is in good agreement with the finite element analysis reported by Byrne et al. [2]. These are based on an effective stress modified Cam clay type model requiring both direct calibration to both measured data and indirect calibration to match the measured undrained shear strength profile [see 20, for details]. In contrast, the AUS model involves a minimum of parameters that can be inferred directly from site investigation data or otherwise estimated in a transparent manner.

7 CONCLUSIONS

A total stress model applicable to clays under undrained conditions has been presented. The model involves three strength parameters: the undrained shear strengths in triaxial compression, triaxial extension and simple shear. The amount of physical anisotropy implied by the model is a function of the relative magnitude of these three strengths. Furthermore, the elastoplastic deformation characteristics are accounted for by a hardening law requiring two additional parameters: the axial strains halfway to failure in triaxial compression and extension. Finally, elasticity, as encountered for example in unloading/reloading, is accounted for by Hooke's law. The result is a relatively simple model whose parameters can all be inferred immediately from standard undrained laboratory tests. The model is applied to a boundary value problem involving horizontal loading of a monopile. The results reveal a considerable influence of the extension and simple shear strengths in addition to the usual compression shear strength. Considering the capabilities of the model along with its relative simplicity and the ease with which it is calibrated to data that can be obtained by standard methods, it appears to be an attractive alternative to more elaborate effective stress models.

APPENDIX 1

Figure 15 of the paper of Ladd [10] shows data of undrained shear strengths in triaxial compression, triaxial extension and simple shear as function of the plasticity index, PI. The trend lines proposed by Ladd are given approximately by:

$$\begin{aligned} s_{ue}/s_{uc} &\simeq 0.50 + 0.0034\text{PI} \\ s_{us}/s_{uc} &\simeq 0.69 + 0.0015\text{PI} \end{aligned} \tag{40}$$

whereby:

$$s_{us}/s_{uc} \simeq 0.47 + 0.44 s_{ue}/s_{uc} \tag{41}$$

The range of plasticity indices covered by Ladd's data corresponds approximately to $0.5 \leq s_{ue}/s_{uc} \leq 0.84$.

In a study concerned with Norwegian clays, Karlsrud and Hernandez-Martinez [5] found the following relations between the strength ratios and the water content w:

$$\begin{aligned} s_{ue}/s_{uc} &= 0.277 + 0.0029w \\ s_{us}/s_{uc} &= 0.454 + 0.00447w \end{aligned} \tag{42}$$

whereby:

$$s_{us}/s_{uc} = 0.03 + 1.54 s_{ue}/s_{uc} \tag{43}$$

for $0.35 \leq s_{ue}/s_{uc} \leq 0.5$ corresponding to the range of water contents considered, $w \simeq 25\%$ to 75%.

References

[1] Burland J. B., Rampello, S. & Georgiannou V. N. & Calabresi, G. (1996). A laboratory study of the strength of four stiff clays, *Proceedings of the Royal Society A*, 254, 1–45.

[2] Byrne, B.W., McAdam, R., Burd, H.J., Houlsby, G.T., Martin, C.M., Beuckelaers, W.J.A.P., Zdravkovic, L., Taborda, D.M.G., Potts, D.M., Jardine, R.J., Ushev, E., Liu, T., Abadias, D., Gavin, K., Igoe, D., Doherty, P., Skov Gretlund, J., Pacheco Andrade, M., Muir Wood, A., Schroeder, F.C., Turner, S. & Plummer, P.A.L. (2017). Numerical modelling of large diameter piles under lateral loading for offshore wind applications, *Proceedings of the Royal Society A*, 254, 1–45.

[3] Byrne, B.W., McAdam, R., Burd, H.J., Houlsby, G.T., Martin, C.M., K. Gavin, P. Doherty, D. Igoe, Zdravkovic, L., Taborda, D.M.G., Potts, D.M., Jardine, R.J., Sideri, M., Schroeder, F.C., Muir Wood, A., Kallehave, D., Skov Gretlund, J. (2015). Field testing of large diameter piles under lateral loading for offshore wind applications, *Proceedings of the XVI ECSMGE, Geotechnical Engineering for Infrastructure and Development*, 1255–1260.

[4] Grimstad, G., Andresen, L. & Jostad, H.P. (2012). NGI-ADP: Anisotropic shear strength model for clay, *International Journal for Numerical and Analytical Methods in Geomechanics*, 36(4), 483–497.

[5] Karlsrud, K. & Hernandez-Martinez, F. G. (2013). Strength and deformation properties of Norwegian clays from laboratory tests on high-quality block samples, *Canadian Geotechnical Journal*, 50, 1273–1293.

[6] Krabbenhoft, K., Karim, M.R., Lyamin, A.V. & Sloan, S.W. (2012). Associated computational plasticity schemes for nonassocited frictional materials. *International Journal for Numerical Methods in Engineering*, 89, 1089–1117.

[7] Krabbenhoft, K. & Lyamin, A.V. (2015). Generalised Tresca criterion for undrained total stress analysis, *Geotechnique Letter*, 5, 313–317.

[8] Optum Computational Engineering (2017). OptumG2: Program for Geotechinical Finite Element Analysis, www.optumce.com.

[9] Optum Computational Engineering (2017). OptumG3: Program for Geotechinical Finite Element Analysis, www.optumce.com.

[10] Ladd, C. C. (1991). Stability evaluation during staged construction, *Journal of Geotechnical Engineering*, 117(4), 540–615.

[11] Potts, D.M. & Zdravkovic, L. (2001). Finite Element Analysis in Geotechnical Engineering, Thomas Telford.

[12] Prashant, A. (2004). Three-Dimensional Mechanical Behavior of Kaolin Clay with Controlled Microfabric Using True Triaxial Testing Triaxial compression and extension test data for a silty clay. PhD diss., University of Tennessee.

[13] Randolph, M. F. (2000). Effect of Strength Anisotropy on Capacity of Foundations, Proc. John Booker Memorial Symposium, Sydney, 313-238.

[14] Roscoe, K.H. & Burland, J.B. (1968). On the generalized stress-strain behaviour of wet clay. In: Engineering Plasticity, Cambridge: 535-609.

[15] Rudnicki, J. W. & Rice, J. R. (1975). Conditions for the localization of deformation in pressure-sensitive dilatant materials, *Journal of the Mechanics and Physics of Solids*, 23, 371–394.

[16] Vardanega, P.J. & Bolton, M.D. (2011). Strength mobilization in clays and silts. *Canadian Geotechnical Journal*, 48, 1485–1503.

[17] Whittle, A.J. (1993). Evaluation of a constitutive model for overconsolidated clays. *Geotechnique*, 43(2), 289–313.

[18] Won, J.Y. (2013). Anistropic strength ratio and plasiticty index of natural clays, Proceedings of the 18th International Conference on Soil Mechanics and Geotechnical Engineering, Paris.

[19] Won, J.Y. (2016). Triaxial compression and extension test data for a silty clay. Personal communication.

[20] Zdravkovic, L., Taborda, D.M.G., Potts, D.M., Jardine, R.J., Sideri, M., Schroeder, F.C., Byrne, B.W., McAdam, R., Burd, H.J., Houlsby, G.T., Martin, C.M., Gavin, K., Doherty, P., Igoe, D., Muir Wood, A., Kallehave, D. & Skov Gretlund, J. (2015), Numerical modelling of large diameter piles under lateral loading for offshore wind applications, *Third International Symposium on Frontiers in Offshore Geotechnics (ISFOG 2015), Oslo, Norway*, DOI: 10.1201/b18442-105 DOI: 10.1201/b18442-105.